

**NASA
Technical
Paper
3264**

1992

**Study of Compression-Loaded
and Impact-Damaged Structurally
Efficient Graphite-Thermoplastic
Trapezoidal-Corrugation Sandwich
and Semisandwich Panels**

Dawn C. Jegley
*Langley Research Center
Hampton, Virginia*



National Aeronautics and
Space Administration
Office of Management
Scientific and Technical
Information Program

Abstract

The structural efficiency of compression-loaded trapezoidal-corrugation sandwich and semisandwich composite panels is studied to determine their weight savings potential. Sandwich panels with two identical face sheets and a trapezoidal corrugated core between them and semisandwich panels with a corrugation attached to a single skin are considered. An optimization code is used to find the minimum weight designs for critical compressive load levels ranging from 3000 to 24 000 lb/in. Graphite-thermoplastic panels based on the optimal minimum weight designs were fabricated and tested. A finite-element analysis of several test specimens was also conducted. The results of the optimization study, the finite-element analysis, and the experiments are presented. The results of testing impact-damaged panels are also discussed.

Introduction

The high stiffness, high strength, low density, and tailorability of composite materials have greatly increased the potential for designing structures which are more efficient than metal structures. An important consideration in designing these structures is the cost involved in their manufacturing. To make composite structures a viable replacement for metal structures, composite structures must be designed to take advantage of cost-effective manufacturing techniques to minimize their cost.

A cost-effective manufacturing technique that is receiving attention is thermoforming. Thermoforming involves the use of constant-thickness graphite-thermoplastic sheets. A structural concept that can exploit thermoforming is a panel with one or two face sheets and a trapezoidal-shaped corrugated core. This structural concept is attractive since the trapezoidal corrugation can be thermoformed from one continuous sheet of material and consolidated into a sandwich panel with two face sheets or a semisandwich panel with one face sheet. The manufacturing process involves thermoforming these large sheets of composite material with metal tools after the sheets have been laid up in the appropriate stacking sequence. Since the corrugated sheet is initially a continuous flat sheet, it is relatively easy to fabricate these panel elements into the desired shape. The corrugations require no additional cutting or aligning; thereby, less effort is required to construct them than discrete stiffeners. However, one drawback to this technique is that thermoforming can impose restrictions on the design if a constant-thickness corrugation is required.

For panels of this type to be used in aircraft structures, they must be structurally efficient, easily man-

ufacturable, and their behavior must be predictable. The present study focuses on examining the response of thermoformed sandwich and semisandwich panels with a trapezoidal corrugation. An analytical optimization study was conducted to identify structurally efficient designs for panels subjected to compressive loads. Results of this study are presented herein. Based on optimal designs, representative panels were fabricated and tested. The results of these tests and of a corresponding finite-element analysis are presented in the present paper. Experimental results for several panels which were impacted prior to compressive loading are also presented.

Panel Configurations and Structural Efficiency Calculations

Two panel configurations were considered in this study. The first configuration is a semisandwich panel with a trapezoidal-shaped continuous corrugation attached to a single face sheet. A cross section of a semisandwich panel is shown in figure 1(a). The second configuration is a sandwich panel with a trapezoidal-shaped continuous corrugation attached to two identical face sheets. A cross section of a sandwich panel is shown in figure 1(b).

Structurally efficient designs were determined for sandwich and semisandwich panels with trapezoidal corrugations. The optimal (minimum weight) configurations were determined and evaluated with the computer code PASCO (ref. 1). The design variables were ply thicknesses and corrugation dimensions. (See fig. 1.) Optimum panels for each configuration were designed to support axial compressive loads corresponding to N_x/L (where N_x is the axial stress resultant and L is the panel length) of 100, 250, 500, and 800 lb/in². No lateral or shear loading was considered.

Allowable stacking sequences contained only $\pm 45^\circ$, 0° , and 90° plies. Design constraints are given in table I and include maximum allowable strains and minimum ply thicknesses on the outermost $+45^\circ$ and -45° plies. The angle between the skin and the sides of the corrugation (fig. 1) was required to be 45° and the skin was assumed to be flat. For the optimization process, all panels were designed to be 30 in. long and 24 in. wide and the material properties for a typical graphite-thermoplastic material given in table II were used. These properties accurately represent the experimentally determined properties of flat graphite-thermoplastic panels as shown in reference 2. Initially, no restrictions were placed on corrugation width (shown as b in fig. 1). Minimum overall extensional and shear stiffness constraints, as given in reference 3, were also included. All panels were designed to be buckling critical; however, the buckling loads determined by PASCO are based on the assumption that no out-of-plane prebuckling deformations are present.

Specimens, Apparatus, and Tests

Panel Configurations

Eleven stiffened panels were fabricated from Hercules AS4 graphite fiber and ICI PEEK thermoplastic resin, and they are described in table III. In each panel, the $\pm 45^\circ$ plies were made with woven fabric and all other plies were made from unidirectional tape. Four types of semisandwich panels and two types of sandwich panels were constructed. The panel designs were based on the PASCO optimization results but significant changes were made to the optimum designs to provide a more realistic design. Changes to the PASCO designs included increasing layer thickness to obtain an integral number of plies (i.e., fractions of plies were rounded up or down), forcing all laminates to be balanced (PASCO requires symmetric laminates), and requiring at least one 90° ply in each laminate. The stacking sequences and dimensions of each fabricated panel are shown in table III. The first letter in the panel designation identifies the geometry and stacking sequence and the second letter identifies the panel as a control or impact-damaged panel. Semisandwich control panels are identified as panels AC, BC, CC, and DC. Sandwich control panels are identified as panels EC and FC. Impact-damaged panels were nominally identical to control panels prior to impact and are identified as panels AI, BI, CI, DI, and EI.

The semisandwich panels were constructed with a flat skin and a corrugation and were placed in the autoclave for consolidation. However, when the panels cooled to room temperature, the skin of the

semisandwich panels deformed out-of-plane into a cylindrical surface. A photograph of the cross section of panel AC is shown in figure 2(a). The amount of curvature of the skin was measured for each panel prior to testing. The variation of the skin from a flat surface (designated as h in fig. 2(a)) was 0.85, 0.42, 0.48, and 0.22 in. for control panels AC, BC, CC, and DC, respectively. The maximum curvature was in panel AC and this curvature corresponds to an equivalent circular cylinder with radius of curvature of the skin of 91 in. The sandwich panels did not deform out-of-plane during the fabrication or cooling processes and were essentially flat. A photograph of the cross section of panel EC is shown in figure 2(b), and an oblique view of panel DC is shown in figure 2(c).

Prior to compression testing, 1 in. of each end of each panel was potted in an epoxy compound and the potted ends were ground flat and parallel. The semisandwich panels were not flattened to remove the curvature prior to potting the ends. Strain gauges were bonded to each panel. The semisandwich panels had strain gauges on the skin and corrugations, whereas the sandwich panels only had gauges on the skins because the corrugation was not accessible enough to apply gauges. The skin of each semisandwich panel and one skin of each sandwich panel were painted white to produce a reflective surface so that moiré interferometry could be used to monitor out-of-plane deformations during the test.

Panel Properties

Two flat coupons 1.5 in. wide, 2 in. long, and approximately 0.2 in. thick were cut from sandwich panel EC after being tested. The coupons were cut from a section of the panel where the corrugation was attached to the skin and where postfailure ultrasonic C-scan inspection indicated that no damage was present. These coupons were loaded in axial compression while the end-shortening displacement was recorded to determine the stiffness of the coupon. Flat coupons could not be cut from the semisandwich panels; thus coupons cut from panel EC are assumed to be representative of all panels tested. Stiffnesses of these coupons were calculated based on load-end-shortening results from the compression tests. Stiffness predictions were also calculated with laminate theory and finite-element analysis with the typical graphite-thermoplastic material properties given in table II. A comparison of the assumed and experimentally determined stiffnesses indicates that the assumed material properties for typical graphite-thermoplastic materials were approximately 25 percent too high to accurately

represent the coupons and the panels tested. Therefore, the experimentally determined stiffness values were used for the finite-element analysis of the test specimens. Equivalent lamina properties corresponding to these stiffnesses are shown in table II. No allowance is made for the fact that all $\pm 45^\circ$ plies were made from woven fabric in all panels tested. These layers are assumed to be tape layers in the analysis (i.e., no fiber undulations were considered). Each flat coupon was measured and weighed prior to testing to determine the density. The assumed density was accurate.

Apparatus and Testing

The five impact-damaged panels were subjected to low-speed impact damage at two locations with a 0.5-in-diameter aluminum sphere projected at speeds up to 450 ft/sec prior to compressive loading. The method described in reference 4 was used for the impact tests. The semisandwich panels identified as AI, BI, CI, and DI were each impacted on the corrugation and on the skin at a speed of 450 ft/sec. Impact sites were located 0.17 times the panel length above and below the horizontal centerline. Sandwich panel EI was impacted on a section of skin not attached to the corrugation at a speed of 250 ft/sec and on a section of skin attached to the corrugation at a speed of 450 ft/sec. Impact sites were located 0.08 times the panel length above and below the horizontal centerline. Impact locations are indicated in figure 2(d).

Control and impact-damaged panels were slowly loaded to failure in axial compression in a 1.2M-lb-capacity hydraulic testing machine. Unloaded edges were unsupported. Strain-gauge data and out-of-plane deformations at selected locations and panel end-shortening displacements were recorded during the test. Moiré fringe patterns were photographed and video taped during the test.

Finite-Element Analysis

A nonlinear finite-element analysis of each control panel was conducted with the STAGS computer code (ref. 5). Actual stacking sequences, measured thicknesses, and corrugation dimensions were used for the analytical model. All plies within a laminate were assumed to be the same thickness, with a woven $\pm 45^\circ$ assumed to be the thickness of two plies. All corrugations were assumed to be identical within a given panel. The entire panel was modeled and the overall panel curvature was included as an initial geometric imperfection. The section of each panel in the potting compound was included in the analytical model and no out-of-plane or lateral deformations

were permitted in this region. The unloaded edges of the panel were unrestrained. Four-node quadrilateral elements were used to model the panels. A uniform grid was implemented along the length of the panel with each element being 1 in. long for panels AC, BC, CC, DC, and FC. Elements which were 0.5 in. long were used to model panel EC. These models involved 6000 to 10 000 degrees of freedom, depending upon panel geometry. The element width varied depending on panel configuration. The boundary conditions for a semisandwich panel are shown in figure 3.

One semisandwich panel was modeled with 1-in-long elements and with 0.5-in-long elements to determine if a converged solution had been obtained. Less than 1 percent difference was found in the end-shortening, prebuckling, and postbuckling out-of-plane displacements or eigenvalues from the analyses based on 1-in-long elements and on 0.5-in-long elements.

The prebuckling stiffness, prebuckling out-of-plane deformation shape, and buckling load were determined for each control panel based on a nonlinear prebuckling stress state. For panels AC and EC, the analysis was continued for loading beyond the buckling load. Nonlinear analysis for the postbuckling response was conducted by using the eigenvector corresponding to the lowest eigenvalue to represent an initial geometric imperfection and to initiate the analysis to determine postbuckling deformation shape and postbuckling stiffness.

Results and Discussion

Optimized Panel Designs

Optimum designs for semisandwich and sandwich panels are presented in this section for a variety of design constraints. In all cases, all four edges of the panel were assumed to be simply supported (PASCO requires simply supported loaded edges) and all corrugations within a panel were assumed to be identical. The initial design imposed no restrictions on the number of corrugations across the panel width of approximately 24 in. However, in each case, the optimum design resulted in five corrugations. Since final optimal designs required exactly a 24-in. width, five 4.8-in-wide corrugations were required. The skin of the panel was assumed to be flat prior to loading for all designs.

The structural efficiency of optimal panel designs, with the typical material properties of graphite-thermoplastic material assumed as shown in table II, was determined. The structural efficiency results are shown in figure 4 in the form of a weight index W/AL

(where W is the panel weight, A is the panel plan-form area, and L is the panel length) versus a load index N_x/L . Results are presented in this manner for ease of comparison with results presented in the literature such as in references 3 and 6. The solid lines represent optimum semisandwich panels and the dashed lines represent optimum sandwich panels. The most structurally efficient configurations are those represented by the lowest curves on the plot, which are those designs with the lowest weight index for a specified load index. The lower dashed and solid curves on the plot were determined by using the constraints in table I. Laminate thicknesses and corrugation width of optimum panel designs using the constraints in table I are given in table IV.

Practical designs would include additional restrictions not included in table I. Examples of such restrictions would be the additional requirement of one 90° ply in each laminate and the requirement of an integral number of plies for each orientation. These additional restrictions were imposed on the designs and the results are also shown in figure 4. These additional requirements increased the weight of the panel 4 to 13 percent above the optimum weight when these additional constraints were not included. Also shown in the figure is the structural efficiency of typical aluminum aircraft panels, represented by the shaded region. The results indicate that the graphite-thermoplastic panels are significantly more structurally efficient than the aluminum panels for all load levels considered. The results also indicate that there is little difference between the structural efficiency of the semisandwich and sandwich panels. The results also indicate that additional constraints which might be required to make the panel designs more practical, such as including a minimum number of 90° plies and an integral number of plies, do not significantly reduce the panel's structural efficiency.

Critical constraints of optimum-design panels are dependent upon design load level and are given in table IV. Extensional stiffness is a critical constraint in all graphite-thermoplastic panels except the most heavily loaded semisandwich panel. Shear stiffness is critical in all semisandwich panels. PASCO cannot calculate an overall shear stiffness for sandwich panels; therefore no overall shear stiffness requirement was imposed on the sandwich panel design. At least one buckling mode is also critical for each panel. Allowable inplane shear strain is a critical constraint for the most heavily loaded semisandwich panel. Optimum corrugation width decreases and height increases as load level increases. The optimal thickness of the $\pm 45^\circ$ and 0° plies depends on load level. The lightest weight panel designs have no 90° plies. For

the lowest load level considered, the thickness of the $\pm 45^\circ$ plies is the minimum thickness allowed.

The structural efficiencies of optimal panel designs in which the constraints in table I were used are shown again in figure 5. The structural efficiencies of optimal panel designs that include all constraints in table I except those on minimum overall stiffnesses and minimum thicknesses of exterior $\pm 45^\circ$ plies are also shown in figure 5. Removing these constraints reduces the weight of the lightly loaded semisandwich panels significantly and has a small effect on the sandwich panel weights. The minimum thickness constraint has little effect on the heavily loaded panels; therefore little difference exists between the heavily loaded semisandwich panels, and no difference exists between the heavily loaded sandwich panels. Sandwich panels are not as structurally efficient as semisandwich panels in some cases because both skins in each sandwich panel were required to be identical, and this resulted in increased weight.

The effects of allowable strains on optimal panel design and structural efficiency of semisandwich panels were examined but are not shown. Allowable axial and lateral strains of 0.003, 0.004, and 0.006 in/in were considered. The allowable strain has no effect on the optimum design of lightly loaded panels but has a significant effect on heavily loaded panels. The lower the allowable maximum strain, the higher is the panel weight for panels designed for load indices greater than 400 psi. However, even the most heavily loaded panels optimized with a maximum strain of 0.003 in/in weigh less than the aluminum aircraft panels.

As mentioned previously, the weight index W/AL and load index N_x/L used for optimization comparisons are the same as those used in previous work. These indices are suited to evaluating trends and comparing panel concepts; however, they do not account for finite-length effects in fabricated panels. The effect of finite panel length on structural efficiency is shown in figure 6 for semisandwich panels 12, 24, and 30 in. long. If the weight index W/AL and load index N_x/L are used, as in figure 6(a), the structural efficiency appears to improve rapidly as the panel length is increased. However, if a weight index of W/A and a load index of N_x are used, as in figure 6(b), the structural efficiency of the panels appears to be far less dependent upon length. Finite-length effects play a significant role in panel design when panels buckle into a mode with only one or two half-waves along the length. To account for these finite-length effects, experimental results are compared by using the weight index W/A .

A comparison between the PASCO and finite-element models and results was conducted for a heavily loaded semisandwich panel by comparing the critical buckling loads predicted by PASCO and by STAGS (using the method described in reference 7). This comparison is only used for model verifications since the allowable boundary conditions in PASCO do not accurately reflect test conditions, since PASCO does not allow for any prebuckling deformations and panel skin curvature is not included in the PASCO analysis. Buckling loads predicted by PASCO and by STAGS for this case differ by less than 5 percent.

Control Panels

The panels described in table III and figures 1 and 2 were loaded to failure in axial compression. A comparison of the test and finite-element results of the control panels is presented in this section. A comparison of W/A and N_x of tested panels indicates that the graphite-thermoplastic panels weigh approximately half the weight of aluminum panels designed to support the same load.

The test specimens described in this section exhibit nonlinear prebuckling deformations. This result is substantiated by the presence of moiré fringe patterns at low load levels that indicate out-of-plane deformations in the specimen skins. Moreover, the semisandwich specimens inherently have load path eccentricity. When these deformation characteristics are present, the onset of buckling is difficult to identify experimentally. Therefore, experimental buckling loads are not presented herein. Analytical buckling loads for the test specimens were obtained by using finite-element analysis. The results are used in the present study to provide insight into the test results. For example, results are presented in figure 7 that show the values of the axial stress resultant N_x in the control specimens at failure, represented by bars in the figure. Analytical predictions of buckling are also shown, represented by symbols. These results suggest that panels BC and DC failed prior to buckling and that the remaining control panels supported load into the postbuckling load range. To gain further insight into panel behavior, selected postbuckling analyses were conducted. A discussion of the test results for each of the panels is presented subsequently.

Semisandwich control panels. The semisandwich specimens exhibited noticeable out-of-plane deformations at low load levels. These deformations were detected by using moiré interferometry. However, the curves for load versus end-shortening were

linear over most of the load range prior to failure and gave no indication of a stiffness change associated with an overall general instability type of buckling response. To gain insight into panel response, buckling and postbuckling finite-element analyses were conducted. The presence of out-of-plane deformations in the test specimens at low load levels motivated the use of buckling analyses that include nonlinear prebuckling deformations.

For panel AC, the global axial stiffness predicted by finite-element analysis is 3 percent less than that of the test specimen. The buckling analysis predicted a localized mode with out-of-plane deformations only in one corner of the panel. Postbuckling analysis indicated a change in the global axial stiffness of less than 1 percent, consistent with the experimental data and the presence of local regions of out-of-plane deformation. A contour plot of the predicted nonlinear out-of-plane prebuckling deformation pattern at a load of 97 percent of the predicted buckling load is shown in figure 8(a). A similar plot of the postbuckling deformation pattern at a load of 161 percent of the predicted buckling load is shown in figure 8(b). These results indicate that the nonlinear prebuckling deformation and postbuckling deformation patterns are very similar in shape and that the bending gradients are much more pronounced in the postbuckling range. The center of the panel has an out-of-plane deformation of 0.06 in. at $P/P_{cr} = 0.97$ and 0.078 in. at $P/P_{cr} = 1.61$, which is just before failure. Both of these deformations are larger than the skin thickness and indicate the presence of large nonlinear bending gradients. Photographs of the panel, showing moiré patterns of out-of-plane deformations, are shown in figures 9(a) and (b) for load levels approximately 95 percent and 170 percent of the predicted buckling load, respectively. These moiré patterns agree with the analytically determined patterns. Out-of-plane deformations are generally confined to regions of the skin where it is not attached to the corrugation and regions near the free edge.

All maximum strains occur in the skin under the corrugation nearest each free edge. The maximum axial and lateral strains occur near the horizontal center of the panel and have values of -0.0055 and 0.0032 in/in, respectively. Maximum shear strains occur at the edge of the potting and have values of ± 0.0022 in/in. Separation at the interface between the skin and corrugation caused the failure of panel AC. As the amplitude of the buckles grew, high strains developed in the skin (at the center of the panel, strain gauges indicated the axial strain was -0.0055 in/in and the lateral strain was 0.0070 in/in at failure) and deformations caused separations at

points where the corrugation meets the skin. A sketch of the initial and deformed cross sections of panel AC is shown in figure 10 (with the magnitude of the deformations amplified). Separation occurred at points labeled A in the sketch. The largest deformations are located in the regions of the skin not attached to the corrugation. Also influencing strains in the panel is the difference in Poisson's ratios between the skin and corrugation. This difference can be expressed as a ratio of the values of the Poisson's ratios in the skin to the value of the Poisson's ratios in the corrugation, as calculated by using laminate analysis. In panel AC, these ratios are $\nu_{xy,skin}/\nu_{xy,corrugation} = 1.3$ and $\nu_{yx,skin}/\nu_{yx,corrugation} = 6.4$. The further these ratios are from 1 (which would represent two laminates with the same Poisson's ratios), the larger is the mismatch in properties and the larger are the interlaminar stresses which develop during loading. This mismatch causes the skin and corrugation to try to deform different amounts even though they are joined together and must maintain deformation compatibility. These resulting high interlaminar stresses eventually result in separation between the skin and the corrugation. A photograph of panel AC after failure is shown in figure 11.

To examine the local deformations under the corrugation, a finite-element analysis of a panel with only one corrugation was conducted. Since the panel skin is less than 0.05 in. thick and contains only one 90° ply, little lateral load is required to induce out-of-plane deformations in the thin skin. Analysis indicates that an applied compressive axial stress resultant induces a tensile lateral stress resultant which is 10 percent of the magnitude of the axial stress resultant away from the clamped edges. However, the applied compressive axial stress resultant induces a compressive lateral stress resultant 60 percent as large as the axial stress resultant near the clamped edges. This compressive lateral stress causes local out-of-plane deformations at the clamped ends, as seen in the tested panel.

Panel BC also exhibited out-of-plane deformations at very low load levels, but the deformation pattern was different from that of panel AC. Prebuckling stiffness predicted by analysis is 3 percent higher than the stiffness found from experiment. The finite-element prediction of prebuckling deformation at $P/P_{cr} = 0.75$ is shown in figure 12, where P_{cr} is the buckling load predicted by finite-element analysis. The moiré pattern just before failure is shown in figure 12(b). No local deformations or high bending gradients of the type seen in panel AC are present. Axial strain gauges indicated strains of -0.0056 in/in at failure. Finite-element analysis also indicates high

axial strain levels at the failure load. Initial failure appears to cause a sudden increase in strain in the corrugation leading to separation between the corrugation and skin. A photograph of panel BC after failure is shown in figure 12(c). The skin and corrugation have separated over a large section of the panel. The difference in Poisson's ratios between the skin and corrugation is less than in panel AC. The ratios of Poisson's ratios are $\nu_{xy,skin}/\nu_{xy,corrugation} = 0.91$ and $\nu_{yx,skin}/\nu_{yx,corrugation} = 0.21$ in panel BC. The panel failed at $P/P_{cr} = 0.88$.

Out-of-plane deformations at very low load levels also occurred in panels CC and DC. Analytically determined prebuckling deformations at $P/P_{cr} = 0.95$ in panel CC and at $P/P_{cr} = 0.88$ in panel DC are shown in figures 13 and 14, respectively. A deformation shape resembling one half-wave in each direction occurred in panel CC just prior to failure. A deformation shape resembling that found in panel BC occurred in panel DC, with the out-of-plane deformation at the unsupported edges opposite in sign from the deformation at the center of the panel. Deformations in panels BC and DC were not limited to the thin section of skin between the corrugations.

The strain gauges at the horizontal centerline of panel CC indicated a maximum axial strain of approximately -0.0055 in/in prior to failure. Strain gauges on panel DC indicated a maximum failure strain of -0.0048 in/in at the panel horizontal centerline on the corrugation. Panels CC and DC failed across the corrugation midlength and the corrugation delaminated from the skin, but little damage in the skin due to panel failure could be seen. The separation between the corrugation and the skin was only at the corrugation-skin interface in panel CC. However, plies from the skin stuck to the corrugation and vice versa in panel DC. Little damage to the skin could be seen after the loading was removed from panels CC and DC. The mismatch in Poisson's ratios between the skin and corrugation is $\nu_{xy,skin}/\nu_{xy,corrugation} = 1.87$ and $\nu_{yx,skin}/\nu_{yx,corrugation} = 5.6$ in panel CC and 1.41 and 2.21, respectively, in panel DC. A photograph of the stiffened side of panel CC after failure is shown in figure 13.

Sandwich control panels. Panels EC and FC also exhibited out-of-plane deformations at very low load levels; however, the magnitude of these deformations remained quite small throughout loading. Predicted and experimental prebuckling stiffnesses differ by less than 1 percent in panel EC but differ by 12 percent in panel FC. Predicted and experimental postbuckling stiffnesses differ by 4 percent in panel EC.

According to the analysis of panel EC, the sections of skin not attached to the corrugations deform prior to buckling, as shown in the contour plot of out-of-plane deflection in figure 15(a). The prebuckling deformation pattern resembles one axial half-wave under each center corrugation. However, the maximum magnitude of the prebuckling deformations is less than one ply thickness. The deformations shown correspond to 94 percent of the predicted buckling load. Moiré patterns indicate that the center sections of thin skin in panel EC deform into a pattern resembling two axial half-waves. However, the skin of the panel was only 0.05 in. thick and the predicted deformation in this region is so small that any imperfection in this section of skin could cause an unexpected deformation shape.

Predicted postbuckling deformations are shown in figure 15(b) for 161 percent of the predicted buckling load. This load corresponds to a value just below that of test specimen failure. Loading was stopped when the attempt to increase load resulted in increased end-shortening and a reduction in load-carrying capability. The failure load was defined as the maximum load level reached. Strains in the panel skins were calculated for this load level. At the maximum load, large deformations occur near the free edges of both skins. The maximum axial and shear strains, -0.0050 and -0.0025 in/in, respectively, occur near the corners of one skin of the panel. Panel EC was ultrasonically inspected by C-scan after testing to determine where damage had occurred since no damage was visible after the panel was removed from the test machine. C-scan inspection indicated that the only damaged region of the panel is a separation between the skin and corrugation at the location of maximum axial and shear strains. The mismatch in Poisson's ratios between the skin and corrugation can be expressed as $\nu_{xy,skin}/\nu_{xy,corrugation} = 1.11$ and $\nu_{yx,skin}/\nu_{yx,corrugation} = 7.79$ in panel EC. According to the analysis, when panel EC reaches a load of $P/P_{cr} = 1.8$, the end-shortening rapidly grows with slight increases in load; this indicates that panel failure would occur.

The deformation shape of one skin and the magnitude of the out-of-plane deformations are shown in figure 15(c). The skins deform by moving toward one another and, therefore, are less likely to cause separations between the skins and corrugation than in panel AC, for example.

Panel FC behaved in a manner similar to panel EC; however, each thin section of skin initially deformed into two axial half-waves, then the entire panel buckled into one axial half-wave. The deformation patterns predicted by analysis indicate out-

of-plane prebuckling deformations of 0.07 in. at the free edges and 0.045 in. in the skin at the center of the panel at a load of 95 percent of the buckling load. The value of 0.045 in. agrees with the experimentally measured value but no measurements were recorded during testing at the panel's unsupported edges. This maximum deformation prior to buckling is larger than the skin thickness. This panel failed by shortening rapidly without additional increase in load but with no visible damage after loading reached a maximum value. C-scan inspection indicated extensive damage near one potted end in a region several inches long and about 10 in. wide. When panel FC reached $P/P_{cr} = 0.99$, the end-shortening rapidly grew and the panel failed. The Poisson's ratios in panel FC are the same as those in panel EC, since the only difference between the panels is length.

Impact-Damaged Panels

One panel of each semisandwich configuration and one sandwich panel were impacted prior to loading. The stiffness and deformation shape of the impacted semisandwich panels differed little from the control panels. The stress resultant and end-shortening (normalized by the panel length) at failure for the control and impact-damaged panels are shown in figures 16 and 17, respectively. Control panels are represented by shaded bars and impact-damaged panels are represented by open bars. The stress resultant of each damaged panel at failure is approximately the same as or lower than the stress resultant of the comparable control panel at failure. However, since end-shortening grows rapidly immediately before and during failure of some panels, the end-shortening behavior may not be a useful way to evaluate the effects of impact damage.

For each panel, impact was severe enough to cause visible damage. An X ray of the impact site on the corrugation in panel AI is shown in figure 18. The damage spread over a region approximately 3 in. long. Impact damage did not affect failure loads in all cases; however, all impact-damaged semisandwich panels failed through an impact site rather than at the location where the control panels failed (at a potted end or midlength). Panel AI failed through the skin impact, whereas panels BI, CI, and DI failed through the corrugation impact.

The progressions of damage during loading are shown in figure 19 for panel AI and in figure 20 for panel BI. The photographs of impact-damaged panels shown in figures 19 and 20 can be compared with those of control panels AC and BC, shown in figures 9 through 12. The impact site is visible prior to loading, as indicated in figures 19(a) and 20(a).

The deformation pattern of panel AI immediately prior to failure is shown in figure 19(b) and resembles that of control panel AC. Little evidence of growth of the impact-damaged area on the skin is seen. The failed panel AI is shown in figure 19(c). The failure loads of panel AC and AI differ by less than 1 percent and the mode of failure is similar. In each panel, the skin and corrugation separated across the width of the panel. The deformation pattern of panel BI immediately prior to failure is shown in figure 20(b) and resembles that of control panel BC. However, evidence of growth of the impact damage area can be seen. The failed panel BI is shown in figure 20(c). The failure loads of panel BC and BI differ by 20 percent, but the mode of failure is similar. In each panel, the skin and corrugation separated across the width of the panel.

Panels CI and DI failed through the corrugation impact site at load levels that are 24 and 3 percent, respectively, lower than those of control panels CC and DC. A photograph of panel CI after failure is shown in figure 21.

Panel EI failed at a clamped end of the panel at a compressive load level within 1 percent of that of the control panel EC. The behavior of panel EI prior to failure was similar to that of panel EC; however, the deformation shape of panel EI more closely resembled that predicted by the analysis than did the deformation shape of panel EC. However, since the magnitudes of these deformations were small, this difference is not significant. Unlike the control panel, the impact-damaged panel failed catastrophically across the entire width of the panel. A photograph of the failed panel is shown in figure 22.

Concluding Remarks

The potential of structurally efficient graphite-thermoplastic panels for aircraft components that were fabricated with the thermoforming technique was examined. Thermoforming can be used to fabri-

cate trapezoidal-corrugation sandwich and semisandwich panels which consist of a continuous corrugation and two or one face sheets, respectively. An optimization study indicates that minimum-weight trapezoidal-corrugation sandwich and semisandwich composite panels are more structurally efficient than current aluminum wing compression panels used on aircraft today. However, semisandwich panels are likely to deform out-of-plane during the fabrication process, which must be taken into account in any design. Testing of semisandwich panels identified a nonlinear displacement behavior; thus, a finite-element analysis based on a nonlinear prebuckling stress state was conducted. This analysis accurately predicts panel deformations and strains caused by axial compressive loading. Analysis indicates that significant prebuckling out-of-plane deformations occurred in all semisandwich panels, as shown by moiré patterns of test specimens under load. Sandwich panels did not deform out-of-plane during fabrication and did not display as much nonlinear behavior as the semisandwich panels. Failure of each control (not impact-damaged) panel involved separation of the corrugation from the skin either near the clamped edge or midlength but always across the entire panel width. Impact-damaged panels failed through the impact site. Failure involved separations of the corrugation from the skin in the impact-damaged panels. Failure loads of impact-damaged panels were as much as 20 percent below those of control panels.

This study indicates that the technique of thermoforming can be used to build structurally efficient graphite-thermoplastic panels and that the prebuckling and postbuckling behavior of these panels can be accurately predicted. Thermoforming is a viable manufacturing technique worthy of further consideration.

NASA Langley Research Center
Hampton, VA 23681-0001
September 18, 1992

References

1. Anderson, Melvin S.; and Stroud, W. Jefferson: A General Panel Sizing Computer Code and Its Application to Composite Structural Panels. *AIAA J.*, vol. 17, no. 8, Aug. 1979, pp. 892-897.
2. Jegley, Dawn C.: *Compression Behavior of Graphite-Thermoplastic and Graphite-Epoxy Panels With Circular Holes or Impact Damage*. NASA TP-3071, 1991.
3. Williams, Jerry G.; Anderson, Melvin S.; Rhodes, Marvin D.; Starnes, James H., Jr.; and Stroud, W. Jefferson: Recent Developments in the Design, Testing and Impact-Damage Tolerance of Stiffened Composite Panels. *Fibrous Composites in Structural Design*, Edward M. Lenoe, Donald W. Oplinger, and John J. Burke, eds., Plenum Press, c.1980, pp. 259-291.
4. Starnes, J. H., Jr.; Rhodes, M. D.; and Williams, J. G.: Effect of Impact Damage and Holes on the Compressive Strength of a Graphite/Epoxy Laminate. *Nondestructive Evaluation and Flaw Criticality for Composite Materials*, R. B. Pipes, ed., ASTM Spec. Tech. Publ. 696, c.1979, pp. 145-171.
5. Almroth, B. O.; and Brogan, F. A.: *The STAGS Computer Code*. NASA CR-2950, 1978.
6. Williams, Jerry G.; and Mikulas, Martin M., Jr.: *Analytical and Experimental Study of Structurally Efficient Composite Hat-Stiffened Panels Loaded in Axial Compression*. NASA TM X-72813, 1976. (Available as AIAA Paper No. 75-754.)
7. Stroud, W. Jefferson; Greene, William H.; and Anderson, Melvin S.: *Buckling Loads of Stiffened Panels Subjected to Combined Longitudinal Compression and Shear: Results Obtained With PASCO, EAL, and STAGS Computer Programs*. NASA TP-2215, 1984.

Table I. Design Constraints

Constraint	Requirement
Panel length, in.	30
Panel width, in.	24
Buckling	Panel does not buckle below design load
Minimum thickness of outer $\pm 45^\circ$ plies, in.	0.0055
Maximum compressive or tensile strain, in/in	0.006
Maximum shear strain, in/in	± 0.01
Minimum global axial stiffness	Dependent upon design load (see ref. 3)
Minimum global shear stiffness	Dependent upon design load (see ref. 3)
Corrugation angle, α , deg (see fig. 1)	45
Corrugation width, b (see fig. 1)	Same for top and bottom
Skins	Same stacking sequence for top and bottom skins of sandwich panel

Table II. Material Properties

Material property	Typical graphite-thermoplastic material	Coupons and fabricated panels
Longitudinal Young's modulus, psi	19.4×10^6	14.5×10^6
Transverse Young's modulus, psi	1.29×10^6	0.97×10^6
Shear modulus, psi	0.74×10^6	0.55×10^6
Major Poisson's ratio	0.38	0.38
Density, lb/in ³	0.057	0.057

Table III. Test Specimens

Specimen designation ^a	Skin stacking sequence	Corrugation stacking sequence	Corrugation width, ^b in.	Panel length, in.
Semisandwich panels				
AC	$[(\pm 45)_2/\overline{90}]_s$	$[\pm 45/0_5/90/0_4/\pm 45]_s$	2.03	12
BC	$[(\pm 45)_2/0_4/90/\pm 45/0_2/90]_s$	$[\pm 45/0_6/\overline{90}]_s$	1.64	12
CC	$[(\pm 45)_3/0_2/90/(\pm 45)_2/0/\overline{90}]_s$	$[\pm 45/0_6/90/0_4/\overline{90}]_s$	1.54	24
DC	$[(\pm 45)_3/0_6/90_2/\pm 45/0_6/\pm 45]_s$	$[\pm 45/0_5/90/0_3]_s$	1.32	24
AI	$[(\pm 45)_2/\overline{90}]_s$	$[\pm 45/0_5/90/0_4/\pm 45]_s$	2.03	12
BI	$[(\pm 45)_2/0_4/90/\pm 45/0_2/90]_s$	$[\pm 45/0_6/\overline{90}]_s$	1.64	12
CI	$[(\pm 45)_3/0_2/90/(\pm 45)_2/0/\overline{90}]_s$	$[\pm 45/0_6/90/0_4/\overline{90}]_s$	1.54	24
DI	$[(\pm 45)_3/0_6/90_2/\pm 45/0_6/\pm 45]_s$	$[\pm 45/0_5/90/0_3]_s$	1.32	24
Sandwich panels				
EC	$[(\pm 45)_2/\overline{90}]_s$	$[\pm 45/0_6/\pm 45/0_6/90]_s$	2.00	12
FC	$[(\pm 45)_2/\overline{90}]_s$	$[\pm 45/0_6/\pm 45/0_6/90]_s$	2.00	24
EI	$[(\pm 45)_2/\overline{90}]_s$	$[\pm 45/0_6/\pm 45/0_6/90]_s$	2.00	24

^aFirst letter indicates panel configuration, and second letter indicates control (C) or impact-damaged (I) specimens.

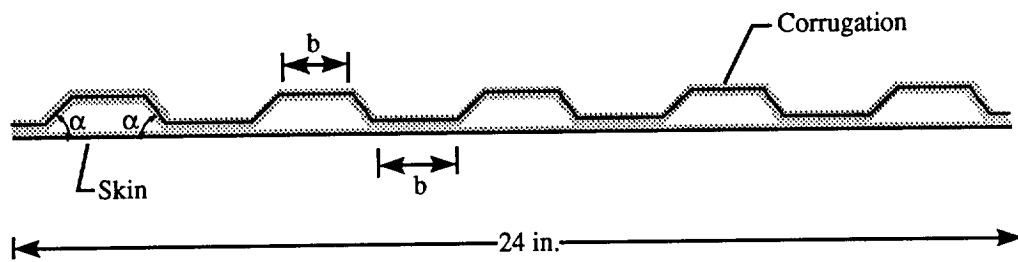
^bCorrugation width is b in figure 1.

Table IV. Optimum Panels

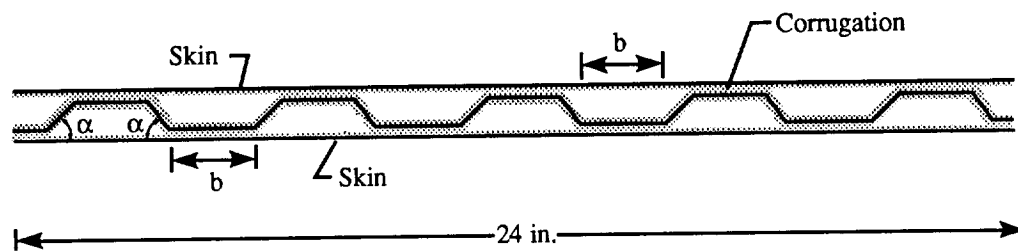
N_x/L , lb/in ²	Critical constraints ^a	Corrugation width, ^b in.	Skin thickness, in.	Corrugation thickness, in.
Semisandwich				
100	E, G, λ_{30}	1.82	0.060	0.112
250	E, G, λ_{30}	1.42	.145	.080
500	$E, G, \lambda_1, \lambda_{15}$.98	.192	.084
800	$G, \lambda_1, \lambda_9, \lambda_{10}, \gamma$.77	.203	.125
Sandwich				
100	$E, \lambda_1, \lambda_{12}, \lambda_{13}$	1.88	0.060	0.049
250	$E, \lambda_1, \lambda_{15}, \lambda_{16}$	1.68	.041	.138
500	$E, \lambda_1, \lambda_{15}$	1.56	.056	.164
800	$E, \lambda_1, \lambda_{12}, \lambda_{13}, \lambda_{14}$	1.21	.077	.166

^a E is the extensional stiffness, G is the inplane shear stiffness, λ_i is the buckling mode with i axial half-waves, and γ is the inplane shear strain.

^bCorrugation width is b in figure 1.



(a) Semisandwich panel.



(b) Sandwich panel.

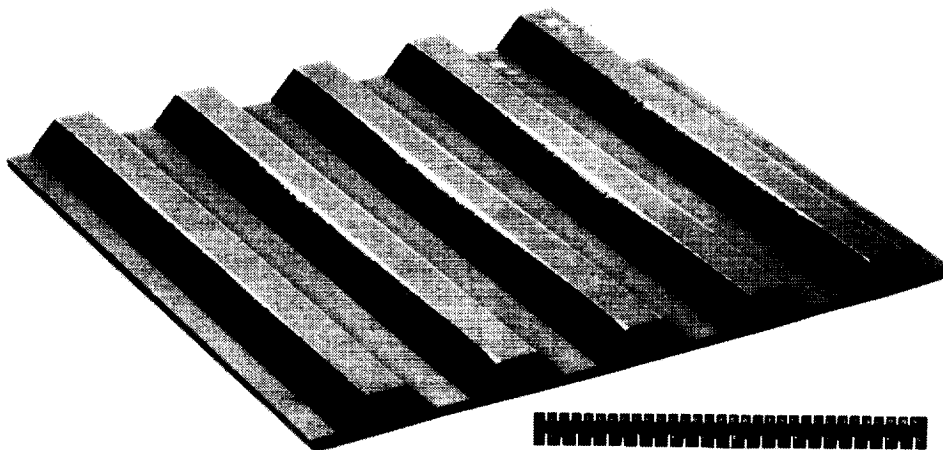
Figure 1. Panel design configurations.



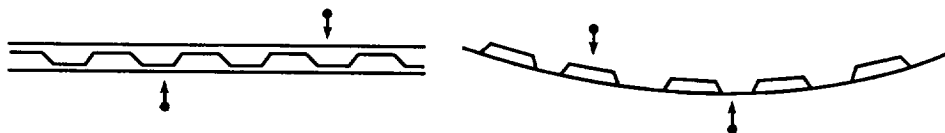
(a) Cross section of panel AC.



(b) Cross section of panel EC.



(c) Panel DC.



(d) Impact locations.

Figure 2. Test specimens.

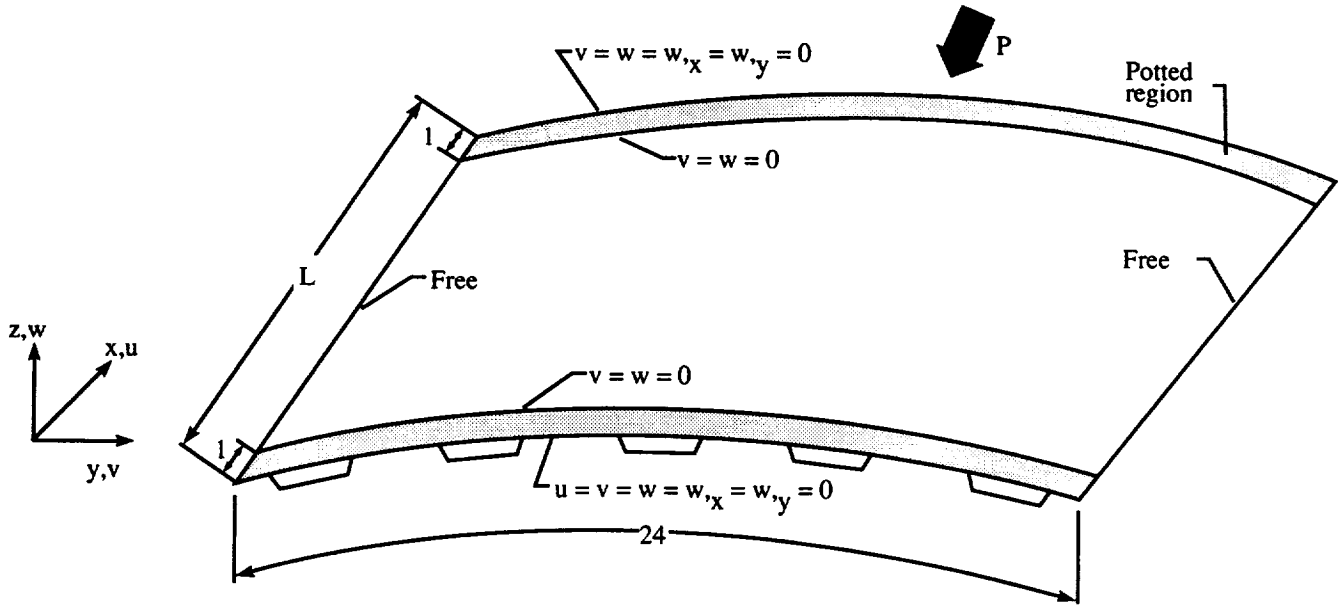


Figure 3. Finite-element boundary conditions. Dimensions are in inches.

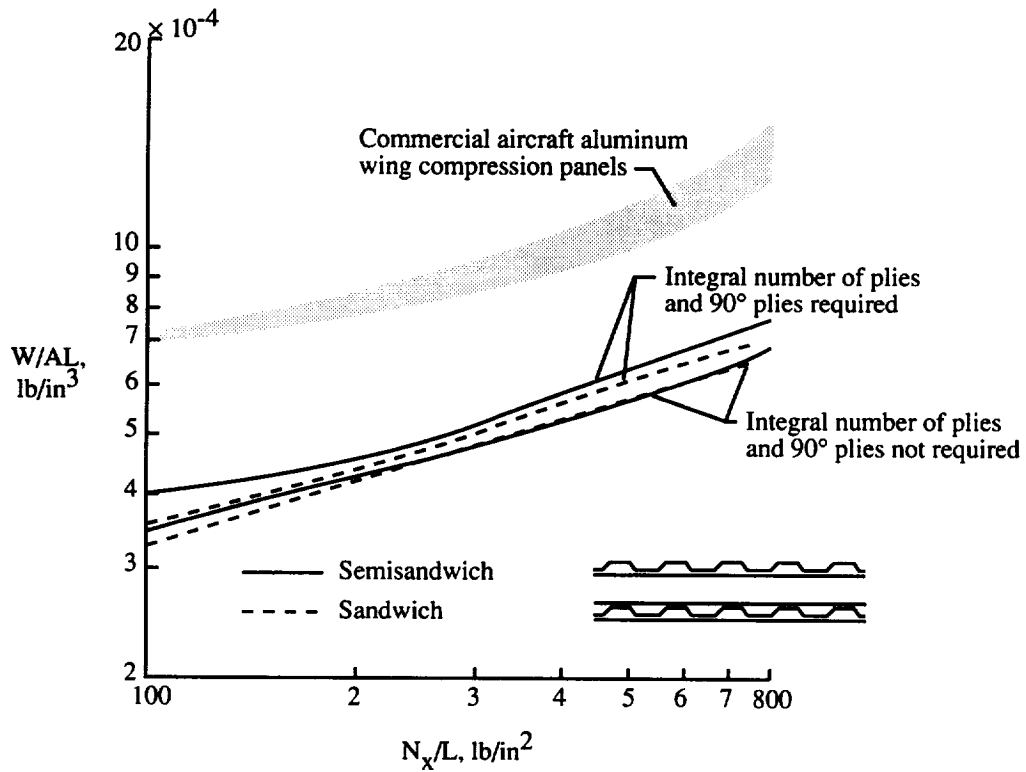


Figure 4. Structural efficiency of graphite-thermoplastic panels.

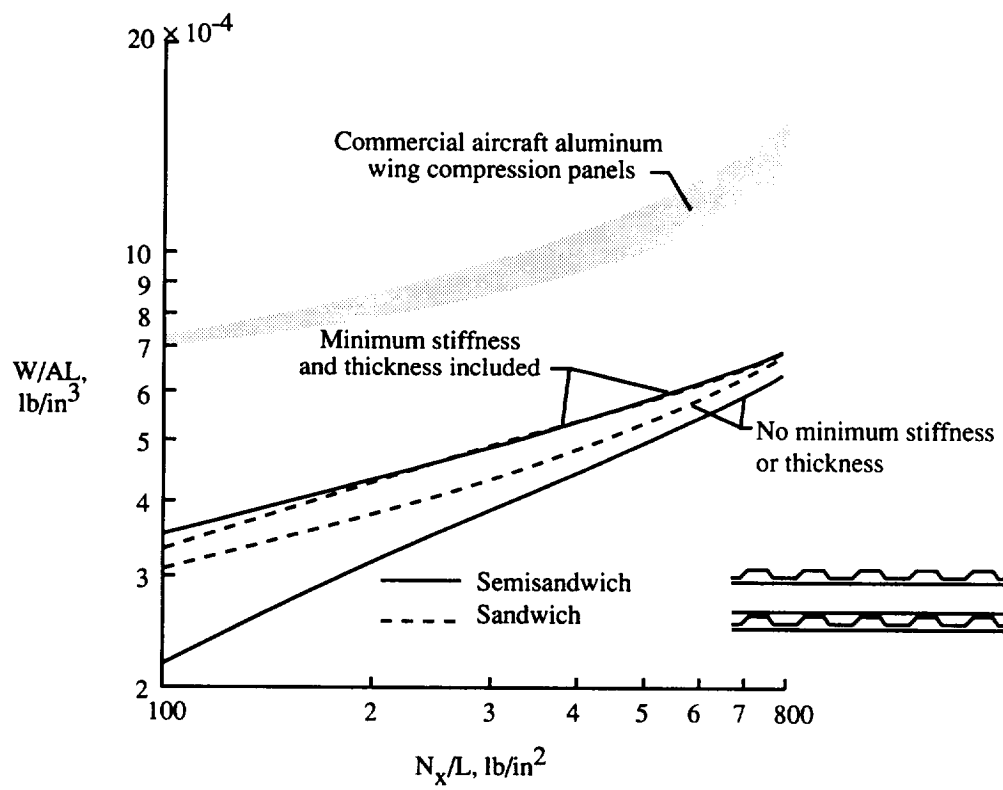
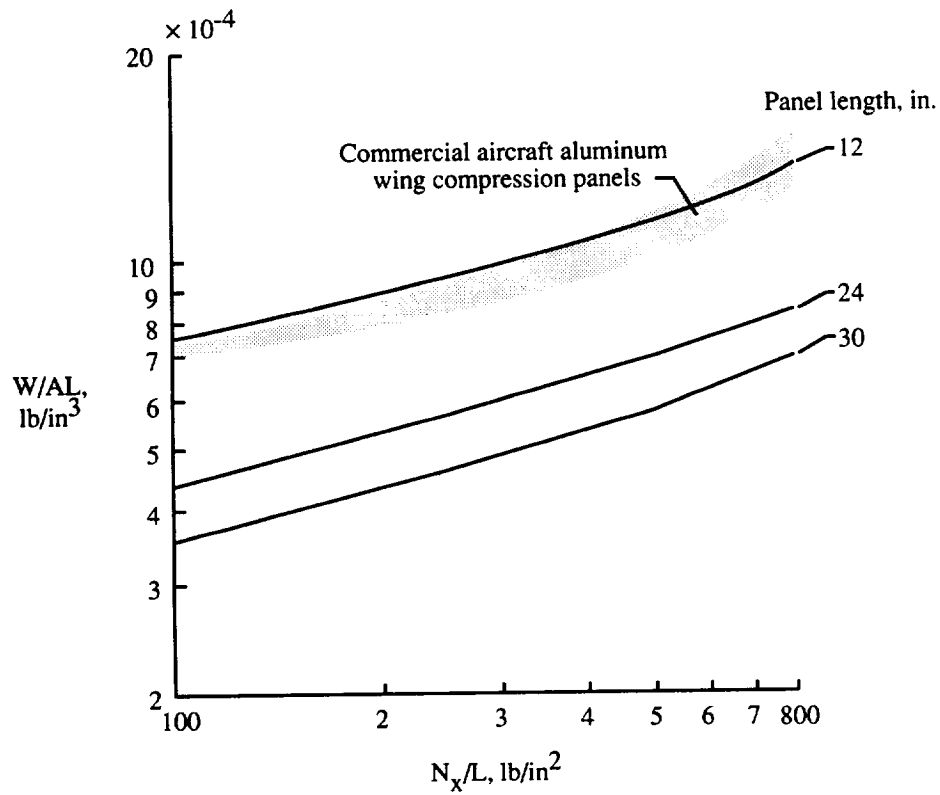
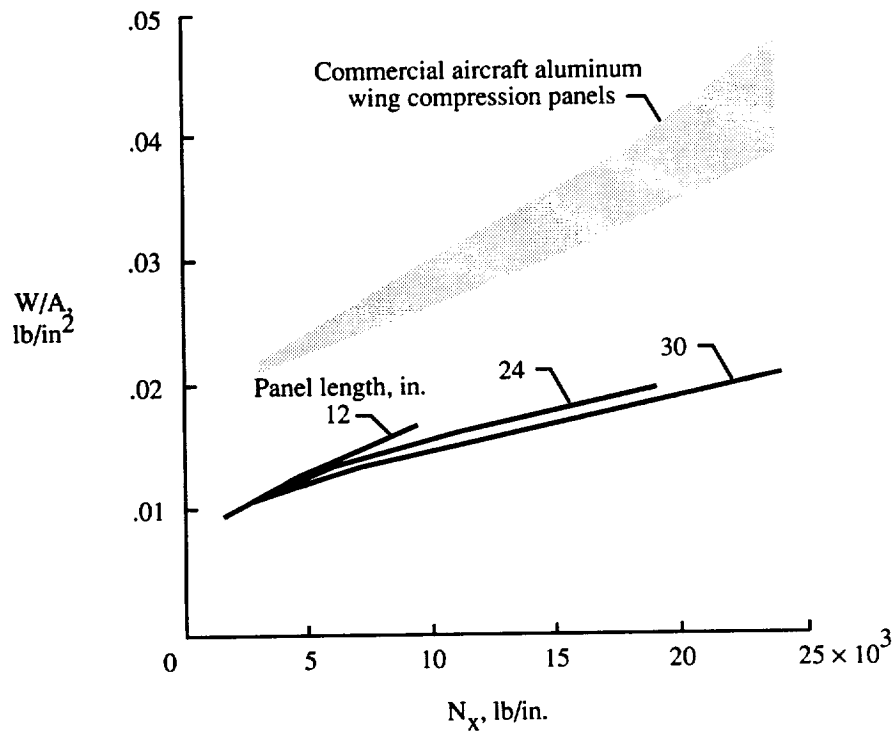


Figure 5. Effect of thickness and stiffness constraints on structural efficiency.



(a) Efficiency expressed with weight index W/AL .



(b) Efficiency expressed with weight index W/A .

Figure 6. Effect of length on minimum weight of semisandwich panels.

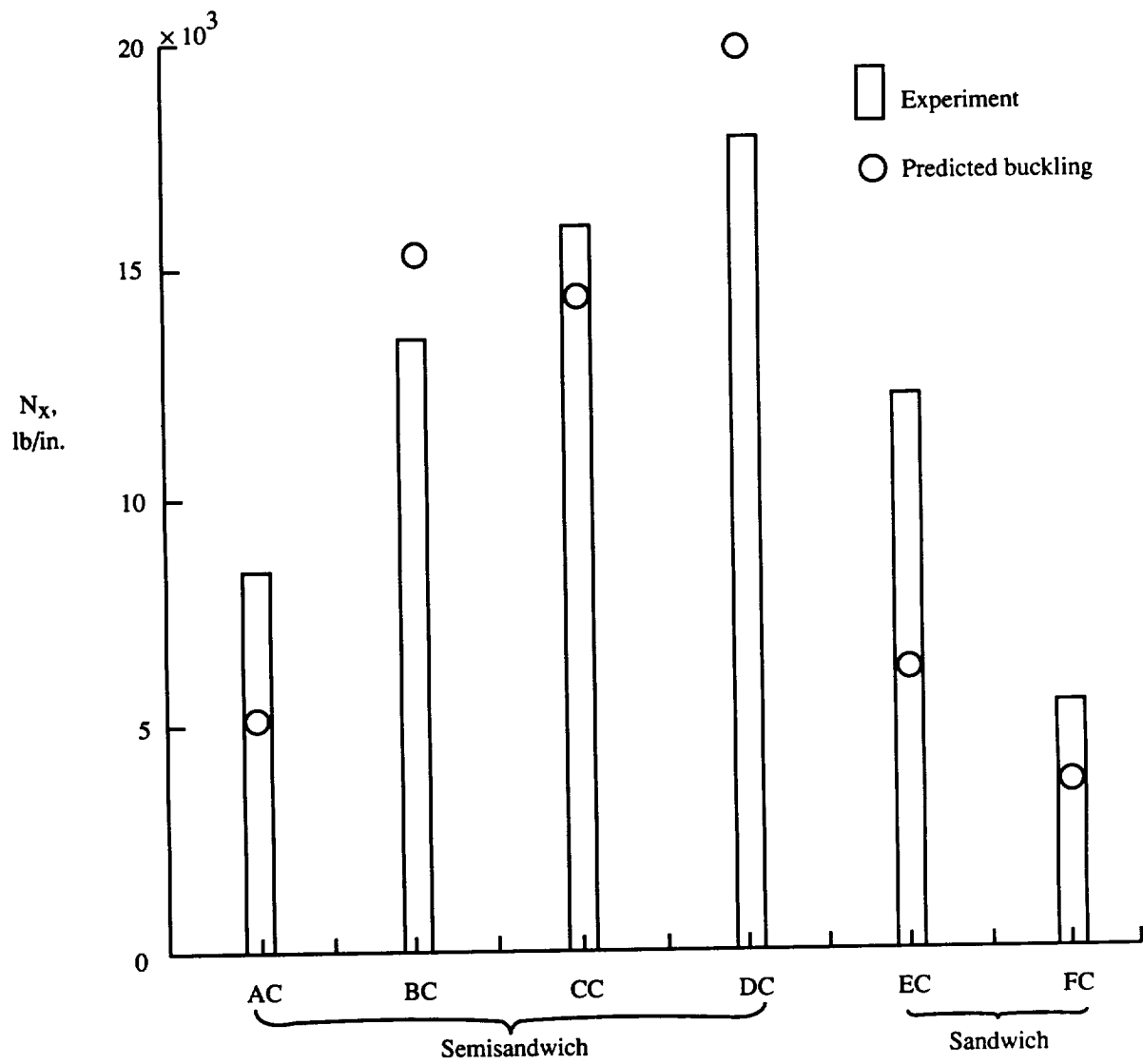


Figure 7. Stress resultants of control panels.

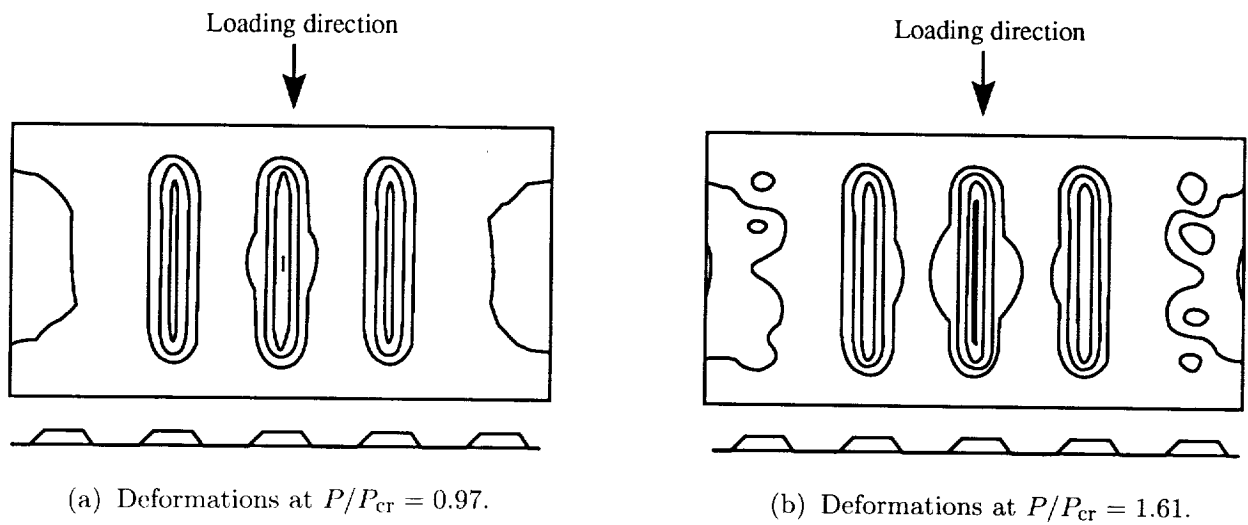
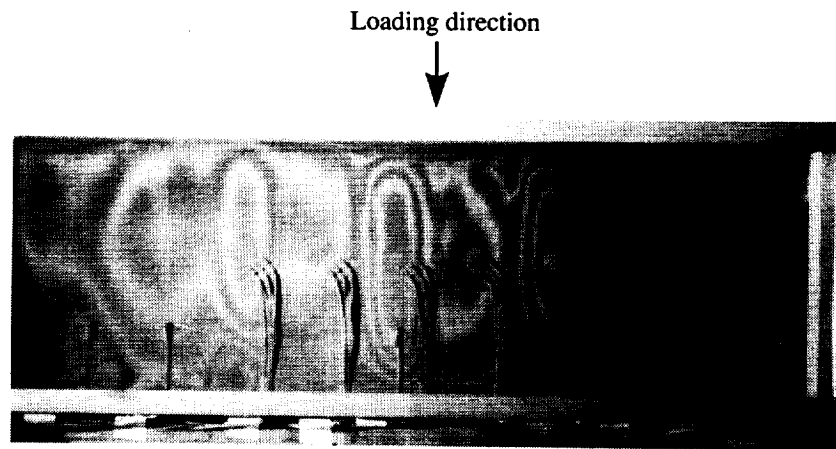
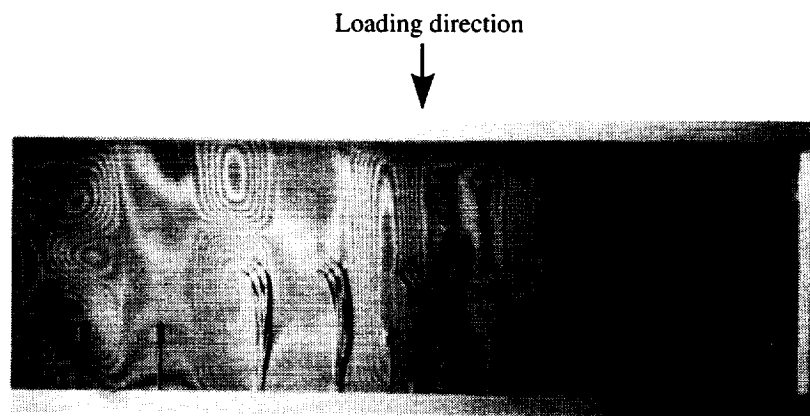


Figure 8. Analytically determined out-of-plane deformations of the skin of panel AC.



(a) Deformations at $P/P_{cr} = 0.95$.



(b) Deformations at $P/P_{cr} = 1.70$.

Figure 9. Moiré patterns of out-of-plane deformations of skin of panel AC.

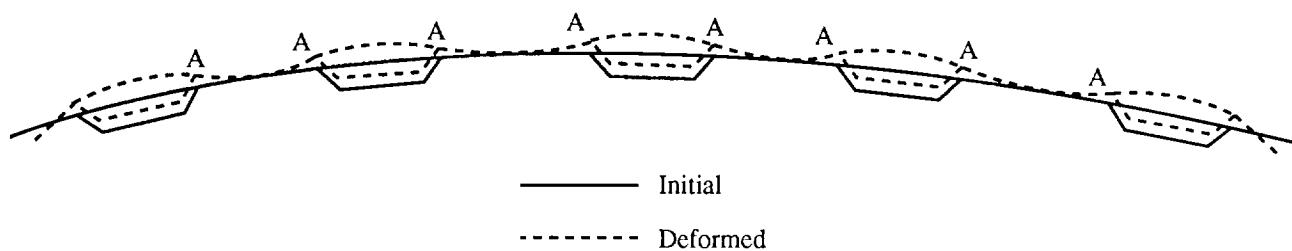
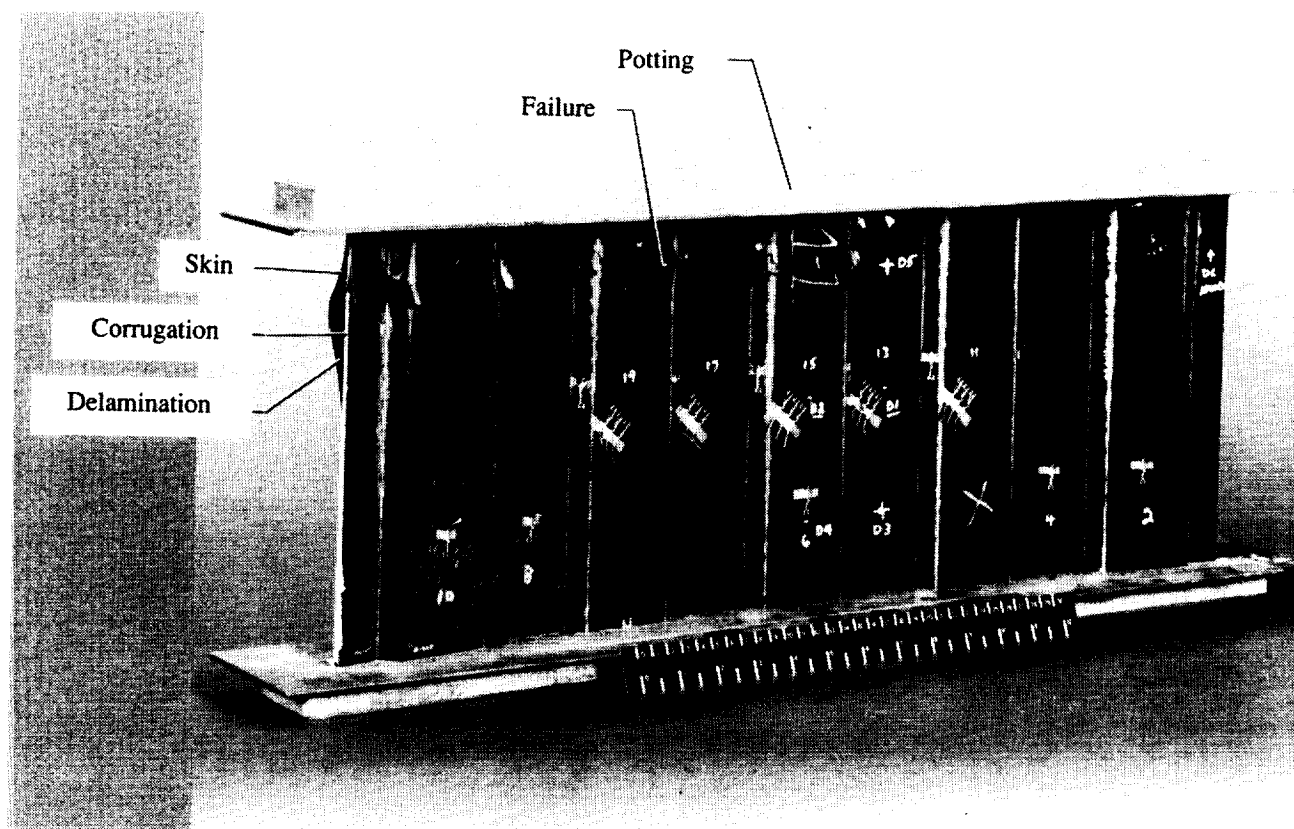
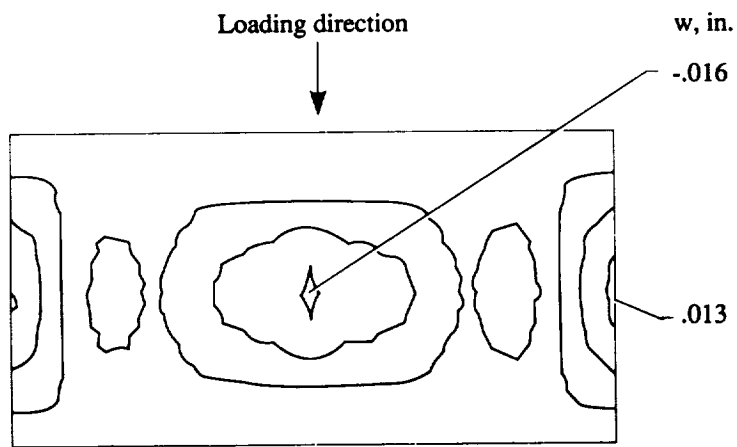


Figure 10. Sketch of deformation shape of semisandwich panel.

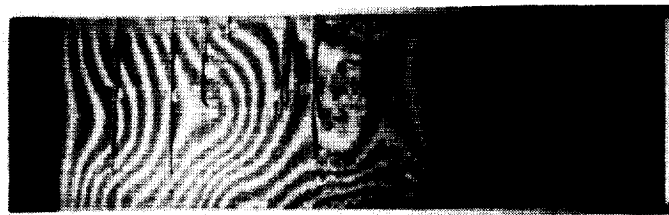


L-92-05015

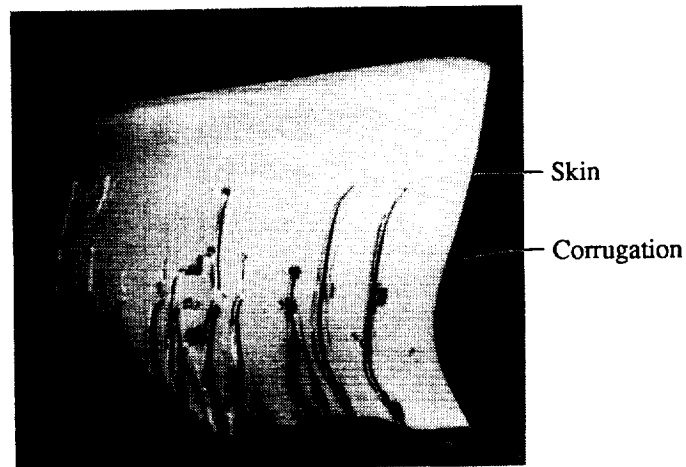
Figure 11. Panel AC after failure.



(a) Deformations at $P/P_{cr} = 0.75$.



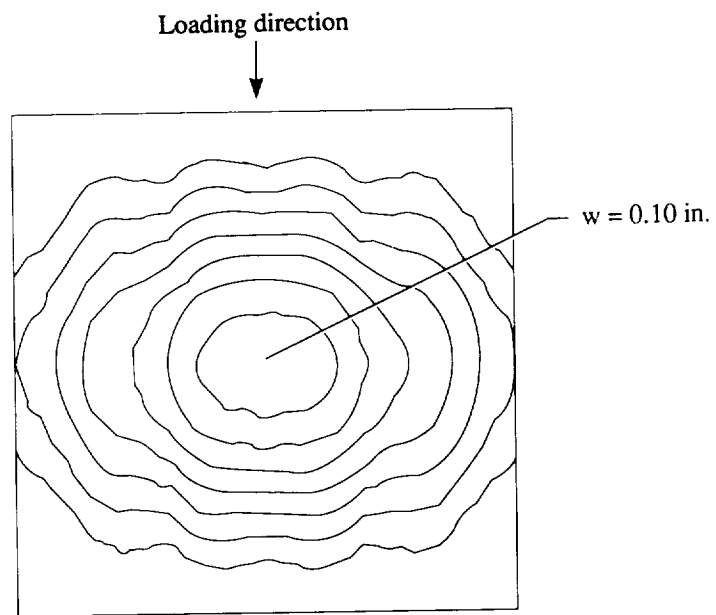
(b) Moiré pattern at $P/P_{cr} = 0.89$.



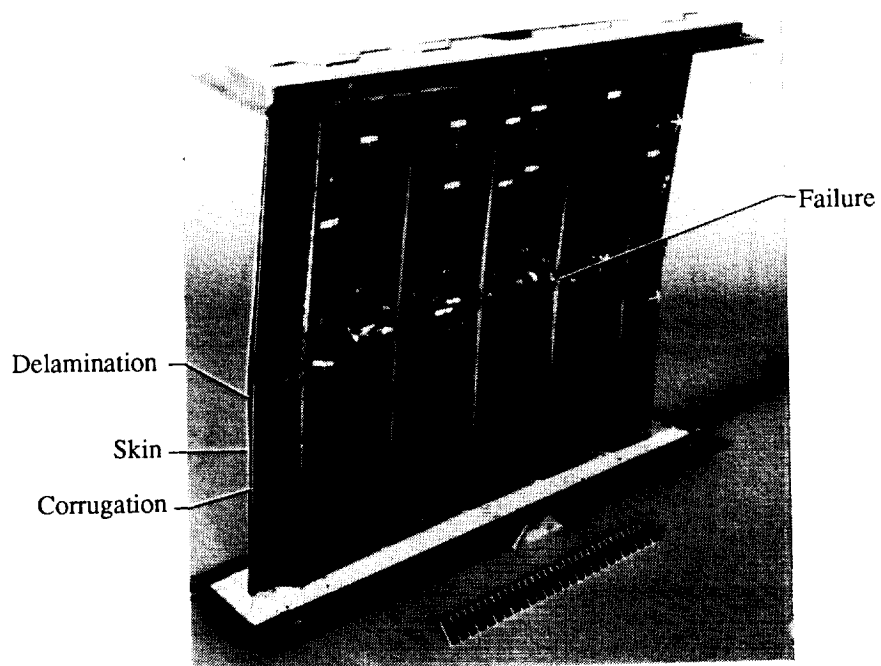
(c) Panel BC after failure.

L-92-05017

Figure 12. Deformations in panel BC during and after loading.



(a) Deformations at $P/P_{cr} = 0.95$.



(b) Panel CC after failure.

L-92-05019

Figure 13. Deformations and failure of panel CC.

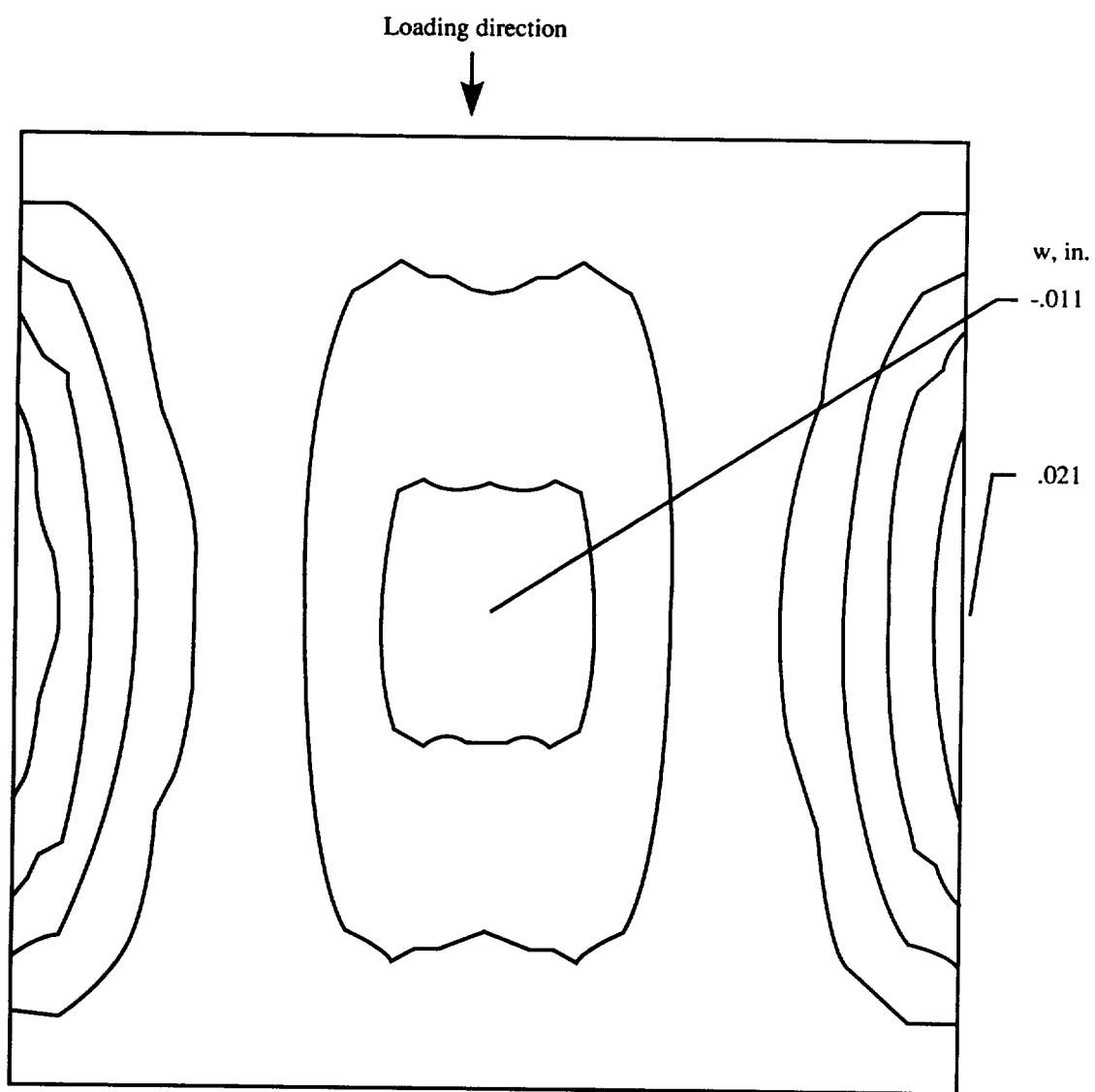
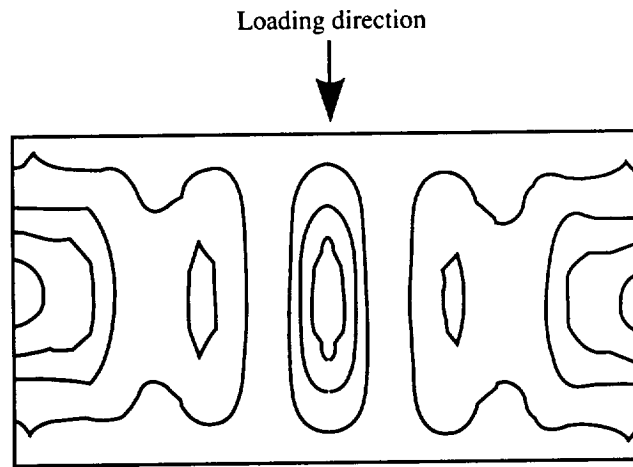
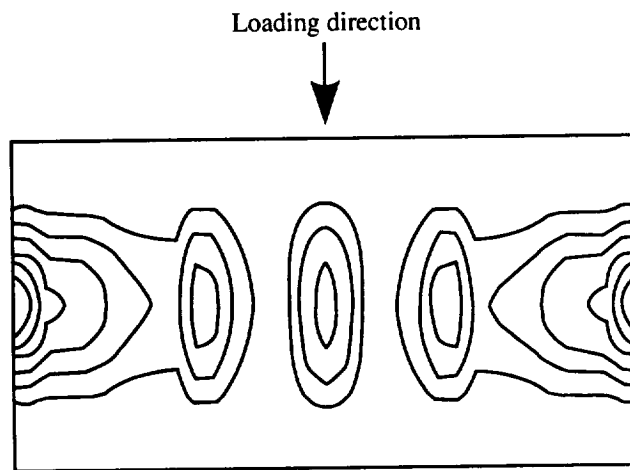


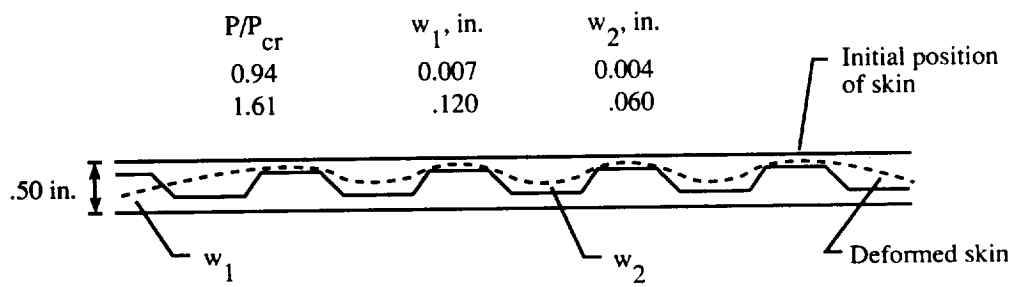
Figure 14. Deformations in panel DC at $P/P_{cr} = 0.88$.



(a) Deformations at $P/P_{cr} = 0.94$.



(b) Deformations at $P/P_{cr} = 1.61$.



(c) Exaggerated deformation shape.

Figure 15. Deformations of one skin of panel EC during loading.

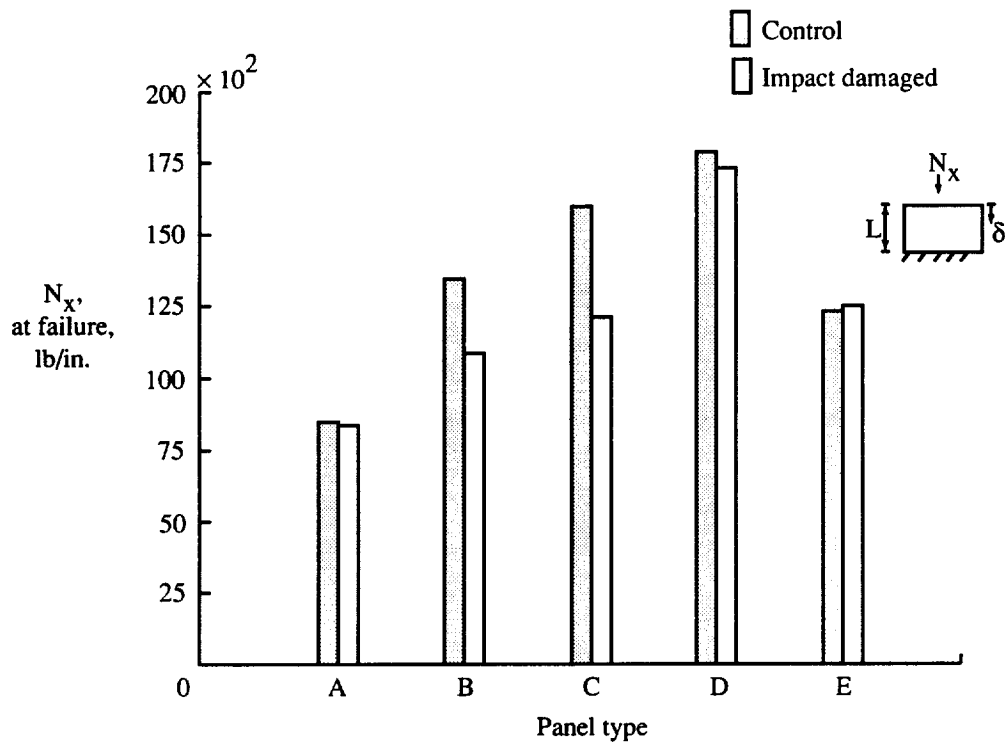


Figure 16. Axial stress resultants at failure of control and impact-damaged panels.

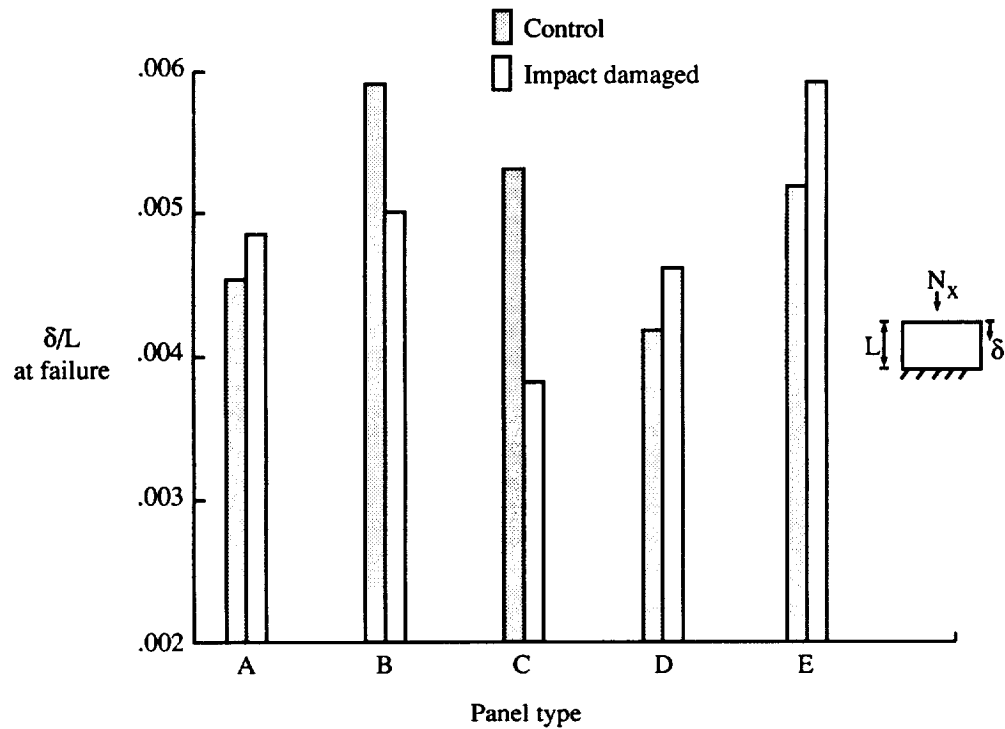


Figure 17. Normalized end-shortening at failure of control and impact-damaged panels.

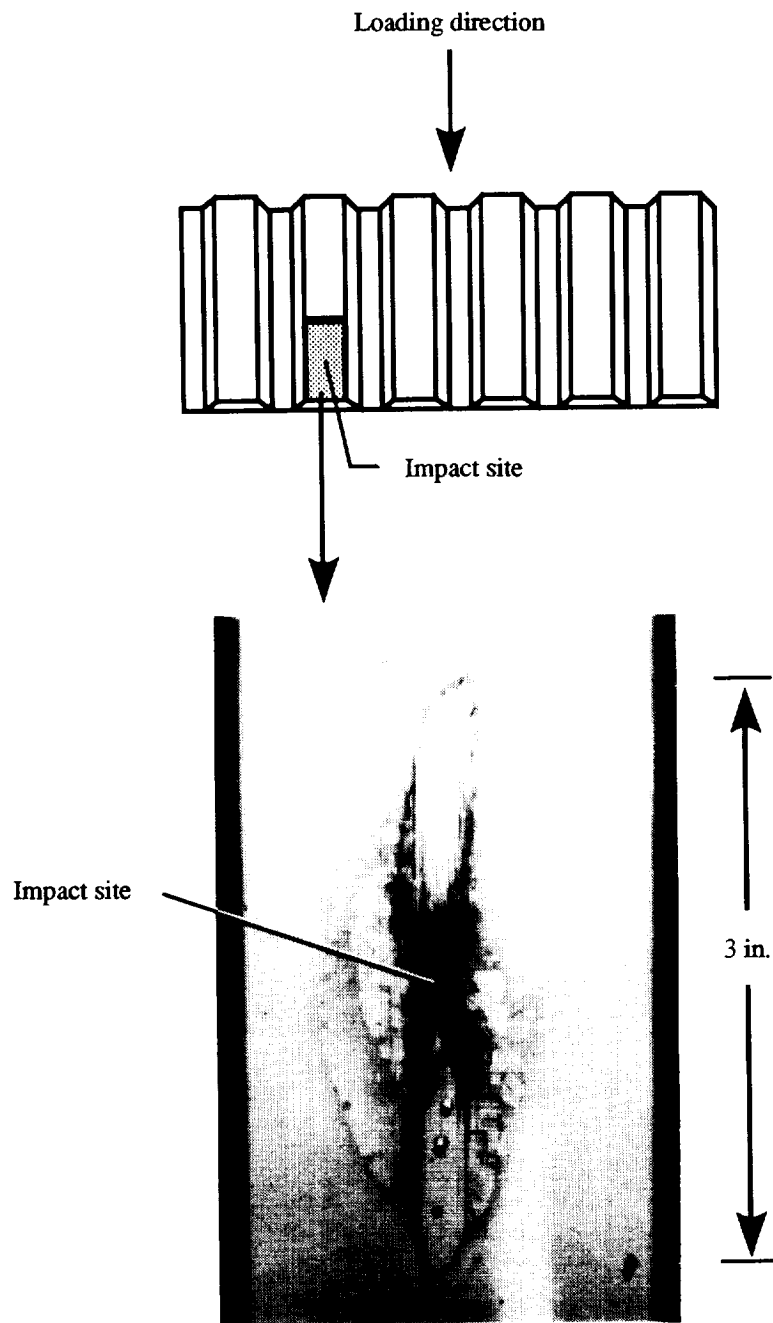
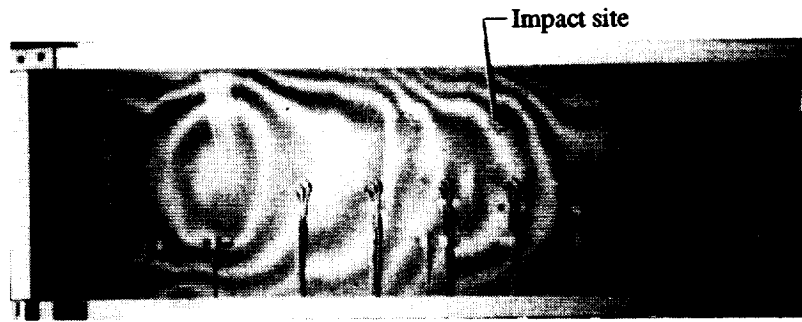
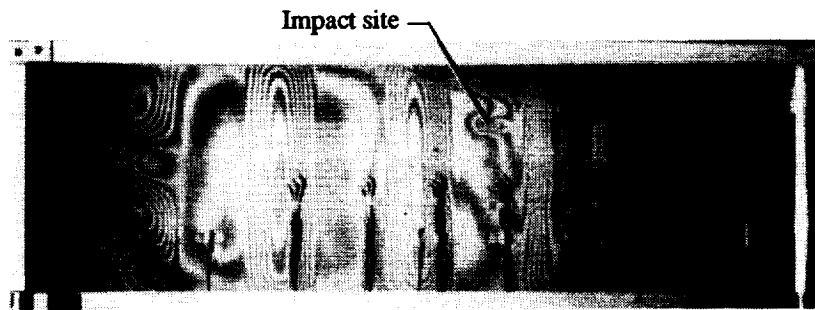


Figure 18. X ray of impact damage to corrugation for impact speed of 442 ft/sec.

ORIGINAL PAGE
BLACK AND WHITE PHOTOGRAPH



(a) Moiré pattern prior to loading.



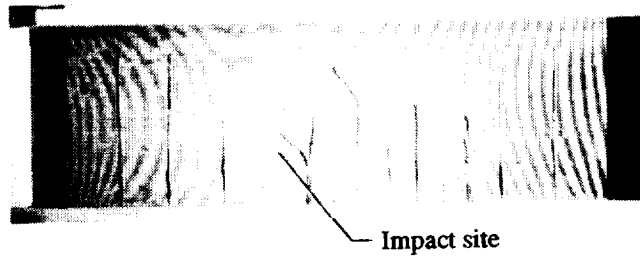
(b) Moiré pattern immediately prior to failure.



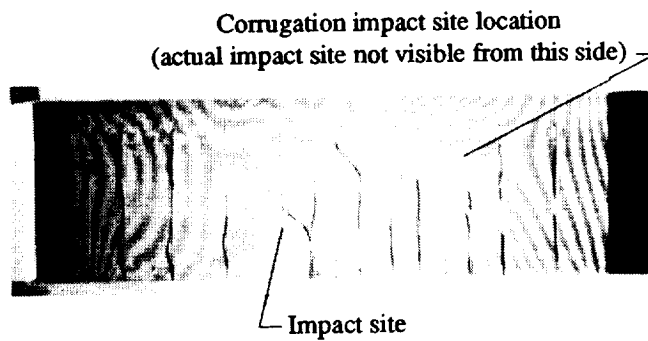
(c) Failed panel.

L-91-2596

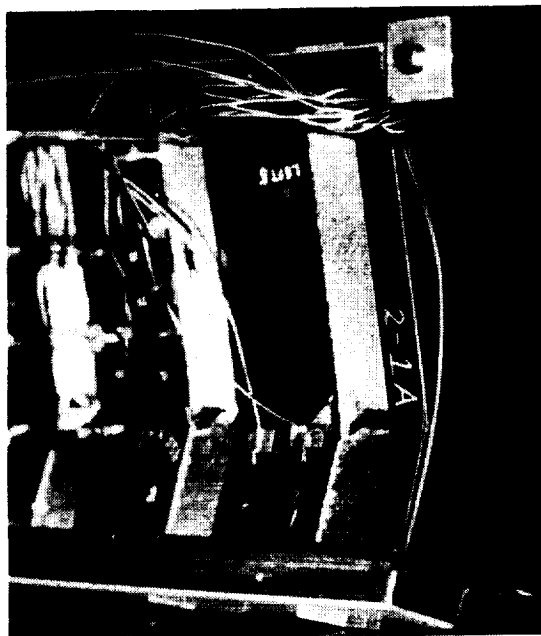
Figure 19. Deformations and failure of panel AI.



(a) Moiré pattern prior to loading.

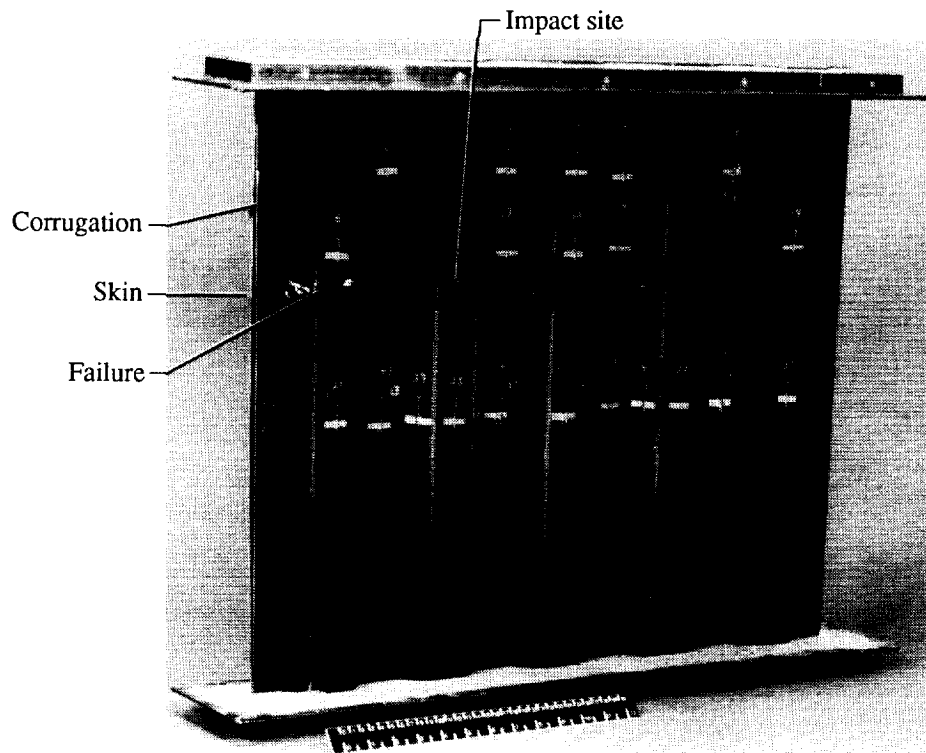


(b) Moiré pattern immediately prior to failure.



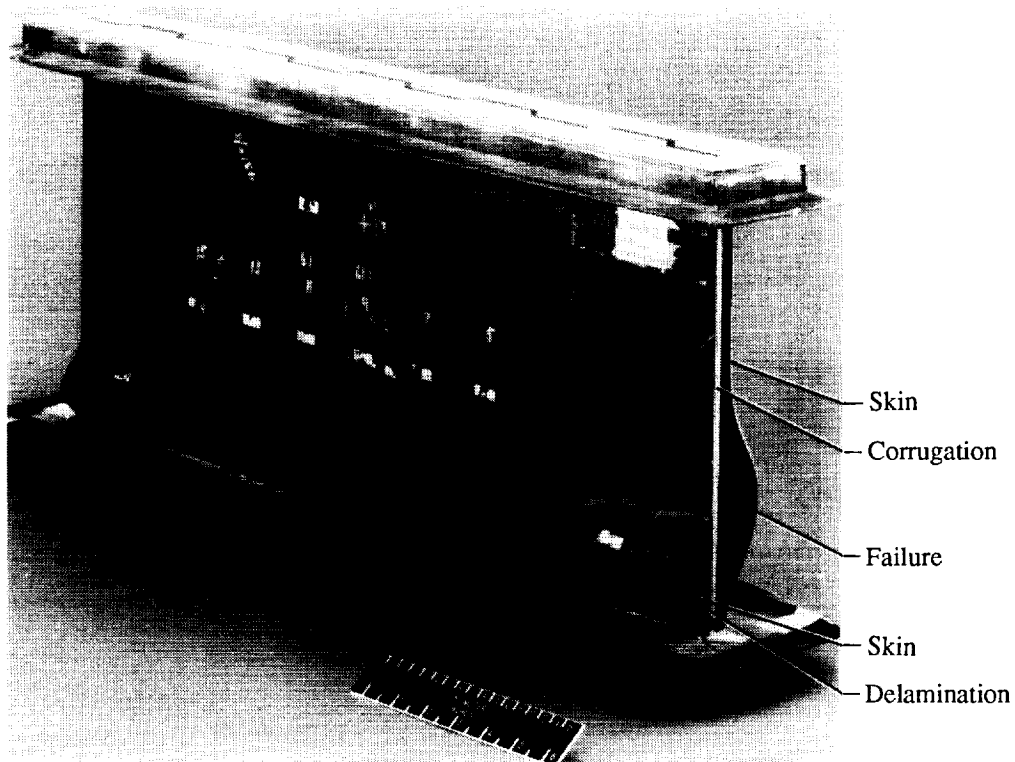
(c) Failed panel. L-92-05020

Figure 20. Deformations and failure of panel BI.



L-92-05016

Figure 21. Panel CI after failure.



L-92-05018

Figure 22. Panel EI after failure.